

SHORT-TERM POSITIONING ACCURACY BASED ON MEMS SENSORS FOR SMART CITY SOLUTIONS

Damian Grzechca, Krzysztof Paszek

Silesian University of Technology, Faculty of Automatic Control, Electronics and Computer Science, Akademicka 16, 44-100 Gliwice, Poland (✉ Damian.Grzechca@polsl.pl, +48 32 237 2717, Krzysztof.Paszek@polsl.pl)

Abstract

The paper presents a method of obtaining short-term positioning accuracy based on micro electro-mechanical system (MEMS) sensors and analysis of the results. A high-accuracy and fast-positioning algorithm must be included due to the high risk of accidents in cities in the future, especially when autonomous objects are taken into account. High-level positioning systems should consider a number of sub-systems such as global positioning system (GPS), CCTV – video analysis, a system based on analysis of signal strength of access points (AP), *etc.* Short-term positioning means that there are other locating systems with a sufficiently high degree of accuracy based on, *e.g.* a video camera, but the located object can disappear when it is hidden by other objects, *e.g.* people, things, shelves *etc.* In such a case, MEMS sensors can be employed as a positioning system. The paper examines typical movement profiles of a radio-controlled (RC) model and fundamental filtering methods in respect of position accuracy. The authors evaluate the complexity and delay of the filter and the accuracy of the positioning in respect of the current speed and phase of movement (positive acceleration, constant) of the object. It is necessary to know whether and how the length of the filter changes the position accuracy. It has been shown that the use of fundamental filters, which provide solutions in a short time, enables to locate objects with a small error in a limited time.

Keywords: electro-mechanical system, received signal strength indicator, positioning, filtering.

© 2019 Polish Academy of Sciences. All rights reserved

1. Introduction

Accurate and fast positioning systems are becoming more important due to new applications and lower costs of devices. The increasing interest in safety in workplaces or autonomous vehicles has led to applications and new solutions in the field of smart cities. There are many approaches to indoor positioning, *e.g.* systems that are based on signals from access points and video cameras [1]. Fig. 1 presents the real problem of (*e.g.* RC model) object location system, which uses and integrates data from the following subsystems: a subsystem of GPS that is used to position objects outside buildings; a subsystem that analyses images from a video camera – it can be used indoors as well as outdoors; a subsystem of *inertial navigation system* (INS) that uses the following three-axis *micro electro-mechanical system* (MEMS) sensors: an accelerometer, a gyroscope and a magnetometer, which also includes a subsystem for object positioning based on the Wi-Fi signal strength – a *received signal strength indicator* (RSSI) that can be used for positioning the object

or for selecting an appropriate camera or group of cameras for the positioning process that is based on the image analysis.

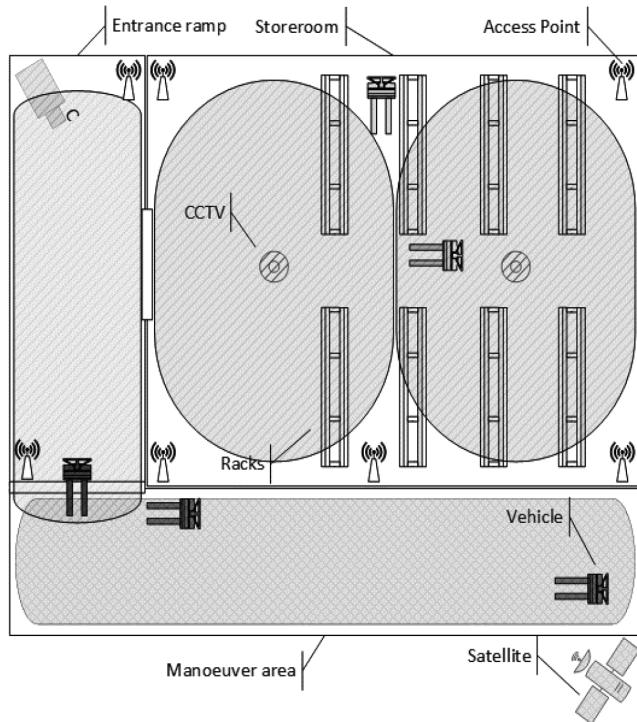


Fig. 1. A model of an object positioning system.

Taking into account the high risk of collisions in narrow corridors or paths in a small area inside a building or in a crowded area outside a building (e.g. a traffic jam) on which vehicles move, a fast, accurate and continuous method of positioning is required. In [2], the authors proposed an algorithm that is used to build a map of obstacles where the known positions of obstacles enable the destination to be reached without collisions. The RC model can be continuously monitored by a high-accuracy subsystem such as a video image analysis one. However, the accuracy of this subsystem depends on the size of the located object, which is very important and must be taken into account. The vehicle size-dependent error can be minimised by using markers (small objects with a specified colour, shape, for example), which are mounted on the vehicles' roofs. Since a vehicle can be covered by other infrastructure elements (e.g. racks), or simply that it can be beyond the sight of the camera, it is necessary to use another subsystem to determine the position of the located vehicle as quickly and accurately as possible. MEMS sensors are becoming more and more accurate and less expensive, and therefore they can be used in vehicles without incurring high costs or introducing major changes in the vehicle structures. Thus, INS subsystems equipped with a fast analysis process can be used in short-term situations in which the position of a vehicle cannot be determined on the basis of a video image. The paper answers the questions at how long a distance (and therefore. time – knowing the speed) can an object be invisible for a video system under various filtration methods and phases of movement and what absolute error is produced? Fig. 2 presents a concept for determining the position using MEMS sensors and

a validation process using data from a video camera. At each of the checkpoints (at time point t_i), the accuracy of the position that is determined by the INS is checked, which enables to find the distance (or time of the movement) in which the error of the determined position is within a given range.

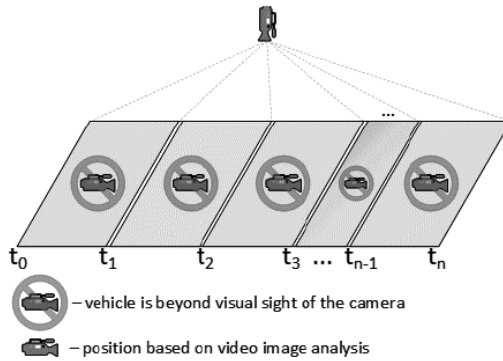


Fig. 2. The correction process based on the data obtained from the video analysis system.

In order to evaluate the proposed method, the following test stand was built: an RC model, a smartphone equipped with MEMS sensors (the subsystem for short-term positioning) and a wireless (WLAN) network adapter (the subsystem to identify a camera or a group of cameras); and a wireless network (WLAN), which are commonly used in buildings and hall infrastructures and in a surveillance camera system.

1.1. Test stand

The test stand was placed in a storage hall that was constructed of metal, glass and brick. The concrete floor had a special rough surface reducing the wheel slippage of the RC model. Fig. 3 presents the structure of the test stand. A video camera was mounted above the centre of the track. The complete track was in the sight of the camera at all times. The track that was used for

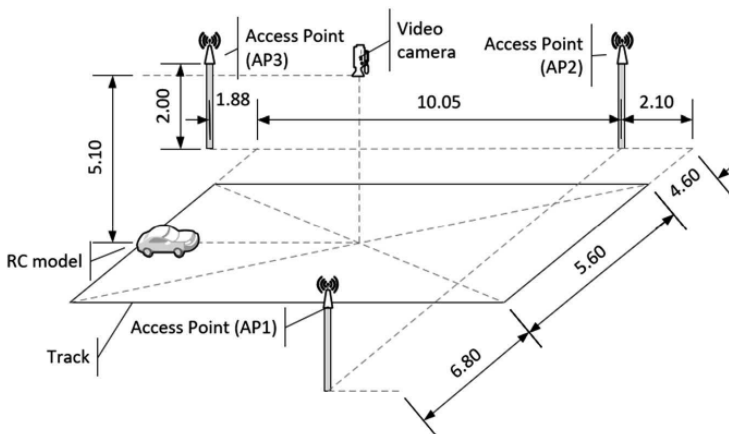


Fig. 3. The test stand structure.

driving was limited in length – 12.15 m and width – 5.60 m. The access points were arranged on a right triangle plan, 2.00 m above the track. Knowledge about materials of the structure of the building as well as the devices that emitted the electromagnetic field was very important because of the MEMS sensors that were used. The electromagnetic field and steel objects influenced the operation of the magnetometer. The environment also affected the Wi-Fi signal, which is similar to that used by the devices that operate on a similar frequency (2.4 GHz).

The bodywork of the vehicle was made of plastic and the frame was made of aluminium and plastic. The driving system of the vehicle consisted of one brush motor, a gearbox and a shaft that transmitted the engine torque to the differentials of both front and rear axles. A turn of the vehicle was made on the front axle of the vehicle using a rudder servo. The RC model was controlled by an RC controller that operated in the 2.4 GHz band. The devices capturing data (a smartphone with MEMS sensors and a wireless adapter) were mounted on the rear spoiler of the vehicle. The smartphone was equipped with an *inertial navigation unit* (IMU) – BMI160 that included an accelerometer and AK09911 containing a gyroscope and a magnetometer. The specifications of the sensors are listed in Table 1.

Table 1. Specifications of the BMI160 and AK09911.

	Accelerometer	Gyroscope	Magnetometer
Sensitivity	2048–16384 LSB/g	16.4–262.4 LSB/(°/s)	0.6 μ T/LSb
Measurement range	± 16 g	$\pm 2000^\circ$ /s	± 4900 μ T
Data rate [Hz]	200	200	50

Rotation of the sensors is very important for the appropriate use of the required equations, especially the signs that are used in them. Fig. 4 shows the rotation of the smartphone and thus MEMS sensors in respect of the RC model.

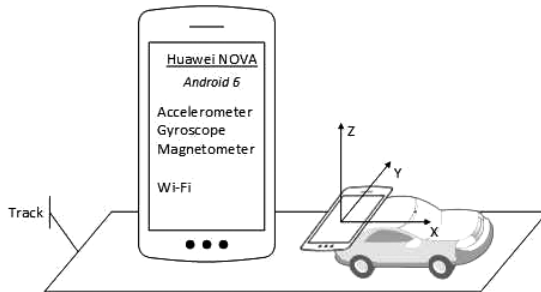


Fig. 4. Rotation of the MEMS sensors.

1.2. Positioning technologies

The technology that is used to determine the position of an object depends on the environment in which the object moves [3]. Preparing the most appropriate technology selection path is difficult and must be balanced between the expected accuracy of the system and its cost. However, in order to obtain a relatively universal system, it is required to use several technologies [4, 5] that are used simultaneously (increasing accuracy) or separately (complementing each other depending on the environment). Fig. 5 shows an example of selection path of the subsystems, which were used separately most of the time.

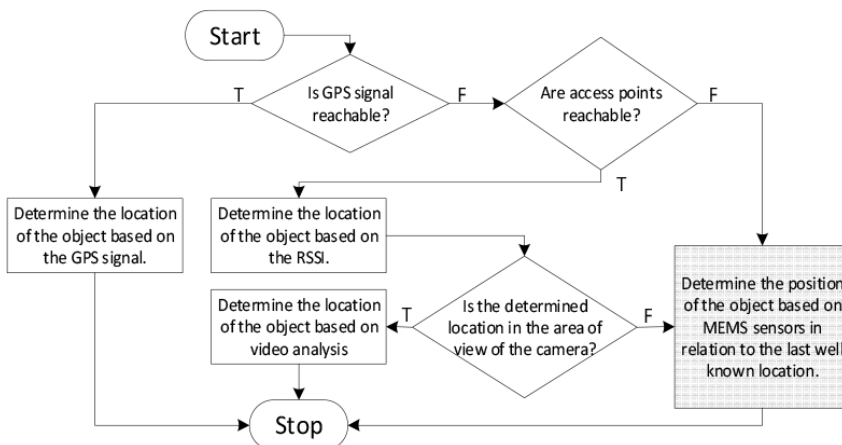


Fig. 5. A flowchart of the system.

2. Position determination

The paper concentrates on the process of determining the position, which is based on the MEMS sensors and the duration of this process, which provides enough accurate information about the position of an object. Additionally, the authors propose an unusual way of positioning that is based on RSSI.

The sample time – T_S is directly associated with the data rate of the sensors. The position of the object is calculated as fast as the fastest INS sensor (accelerometer and gyroscope) produces data at the output, which for our device means that the sample time is equal to 0.005 s – the data from the magnetometer are delivered four times slower, and therefore the remaining data are approximated, *i.e.* kept at the previous level. Due to the use of several positioning subsystems, synchronisation of the data streams was required. The synchronisation process was performed manually at the beginning of each test scenario.

2.1. Reference system

The reference data (object positions) were obtained by analysing the video images. A sequence of images was recorded using the video camera that was located above the centre of the movement area of the object. The video camera that was used enabled images to be recorded at a speed of 30 fps. The object was detected and located using the *centre of mass* (COM). The position (in pixels) in an image was transformed to the position in the coordinate system that was used.

It must be noted that the reference data were burdened with errors that resulted from the COM of RC model being located (which was 0.52 m long and 0.33 m wide) and the speed of video recording (30 fps). In the worst case, these errors were 0.30 m and 0.07 m (assuming an object speed of 2.1 m/s), respectively. This meant that the position that was obtained using the MEMS sensors was compared with the reference data with an accuracy of 0.30 ± 0.07 m.

2.2. Position determination based on MEMS sensors

In order to determine the position of a vehicle that is based on the data obtained from MEMS sensors, the following actions are performed: data filtration, followed by determination of velocity,

distance and movement direction. The filtration is performed by using fundamental algorithms with a moving window (moving average (A) [6, 7], median (M) [6, 8], Savitzky–Golay (SG) [9], Hampel (H) [10]) or their combinations. The value of velocity v of an RC model is determined based on the accelerometer readings and is calculated using (1) from the values of: v_0 – initial speed [m/s]; $a(t)$ – acceleration [m/s²]; t_0 – time at the starting point [s]; t_N – time at the final point [s] and T_S – sampling time. After that, the travelled distance s is calculated using (2).

$$v = v_0 + \sum_{t_i=t_0}^{t_N} a(t_i) \cdot T_S, \quad (1)$$

$$s = \sum_{t_i=t_0}^{t_N} v(t_i) \cdot T_S. \quad (2)$$

In order to obtain the coordinates of the vehicle, the information about the direction of the RC model movement is also required. The direction is obtained from the magnetometer and accelerometer. The azimuth ϕ_A can also be determined based on the data that are obtained only from the magnetometer (X axis – m_X , Y axis – m_Y , Z axis – m_Z) (3). However, in order to increase the azimuth accuracy, the determination of pitch (4) and roll (5) (Fig. 6) of the vehicle should be taken into account (a_g – gravity) [11]. The corrected values from the magnetometer, after considering the rotation of the sensors, are calculated using (6) and should be used in (3) [12]. Additionally, in order to obtain values from 0 to 360 degrees, the constraints of the arctan function must be taken into account (by checking the sign of the corrected values from the magnetometer), as is shown in (7):

$$\phi_A = \arctan\left(\frac{m_Y}{m_X}\right), \quad (3)$$

$$\phi = \arctan\left(\frac{a_{gX}}{\sqrt{a_{gY}^2 + a_{gZ}^2}}\right), \quad (4)$$

$$\theta = \arctan\left(\frac{a_{gY}}{\sqrt{a_{gX}^2 + a_{gZ}^2}}\right), \quad (5)$$

$$\begin{cases} m_{X_h} = m_X \cdot \cos(\phi) - m_Y \cdot \sin(\theta) \sin(\phi) + m_Z \cdot \cos(\theta) \sin(\phi) \\ m_{Y_h} = -m_Y \cdot \cos(\theta) - m_Z \cdot \sin(\theta) \end{cases}, \quad (6)$$

$$\phi_A = \begin{cases} 90 & \text{for } m_{X_h} = 0 \wedge m_{Y_h} < 0 \\ 270 & \text{for } m_{X_h} = 0 \wedge m_{Y_h} > 0 \\ 180 - \arctan\left(\frac{m_{Y_h}}{m_{X_h}}\right) \cdot \frac{180}{\pi} & \text{for } m_{X_h} < 0 \\ -\arctan\left(\frac{m_{Y_h}}{m_{X_h}}\right) \cdot \frac{180}{\pi} & \text{for } m_{X_h} > 0 \wedge m_{Y_h} < 0 \\ 360 - \arctan\left(\frac{m_{Y_h}}{m_{X_h}}\right) \cdot \frac{180}{\pi} & \text{for } m_{X_h} > 0 \wedge m_{Y_h} > 0 \end{cases}. \quad (7)$$

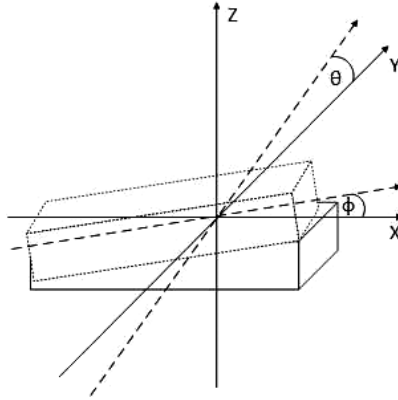


Fig. 6. The roll and pitch angles.

2.3. Position determination based on RSSI

In order to determine the position of vehicles in 2D floor plans that is based on *RSSI*, the following actions should be performed: selection of three access points that are within a given range, calculation of the distances between the vehicle and selected access points and minimisation of the mean square error of the estimated position.

The distance between the RC model and a single access point is determined based on the wave propagation model. However, a number of factors influence the function, and therefore the accuracy of the positioning is seriously limited [13]. By knowing the path loss component η , which is experimentally selected, and the received signal strength $RSSI_0$ in the reference distance r_0 it is possible to calculate the distance r based on the value of the *RSSI* using (8) [14]:

$$r = r_0 \cdot 10^{\frac{RSSI_0 - RSSI}{10\eta}}, \quad (8)$$

In the model case, the vehicle is at the intersection of three circles, the centres of which are in mounting points of the APs, and the radii are determined based on the *RSSI*. In this situation, the coordinates of the RC model can be calculated using a very simple system of three circle equations. However, in practice, the designated circles do not intersect at one point (sometimes, there is no common point). In order to determine the position of the vehicle, minimisation of the mean square error is performed, according to (9), where r_i – the calculated distance; r'_i – the estimated distance and n – the number of access points [15]:

$$\sigma^2 = \frac{1}{n} \sum_{i=1}^n (r_i - r'_i)^2. \quad (9)$$

In order to find the solution to (9), the Nelder-Mead simplex algorithm [16] was used (the built-in MATLAB function used to find the minimum of a given function). The starting point (initial position) was the centroid of a triangle that was built on three selected access points, although it could also be a previous position of the object. The stop criterion is the number of iterations, which may depend on hardware, speed of the vehicle or expected error. For the requirements of this study, the stop criterion was the maximum number of iterations, which was a constant value of 40.

3. Research result

During the tests, two models of movement were selected: MA and MB. The characteristics (time and speed) of each phase (acceleration and constant motion) of the movement for each model are presented in Table 2. The track of the movement was a 12 m straight line.

Table 2. Two examined motion cases.

Motion	Accelerated $a > 0$		Constant $a = 0$	
Model	Time [s]	Speed [m/s]	Time [s]	Speed [m/s]
MA	1	3.8–5.8	0	–
MB	2	1.3–2.1	2	2.0–2.2

It should be taken into account that the use of a filter with a moving window results in an output signal that is delayed by the time (t_D) that is required to receive the data for half of the window width – K (10). For example, the data filtered by A_49 were delayed by 0.12 s.

$$t_D = \left\lfloor \frac{K}{2} \right\rfloor \cdot T_S \tag{10}$$

3.1. Constant-motion phase

The relationship between the absolute position error (Δ_p) and the distance travelled in the constant-motion phase (see Table 2) in the MB model is presented in Table 3. The first column contains the applied filtration (according to the pattern – {filter type}_{window width}) of velocity, the second column contains the distance travelled by the object (for the filtration that was used) with a position error of up to $\Delta_p = 0.05$ m, the third column contains the distance travelled by the object with a position error of up to $\Delta_p = 0.1$ m, etc. If the contents of the last columns in the table are “–”, it means that the RC model reached the final distance of the measured range. When interpreting the values from this table, the absolute position errors increased with the distance (time of the movement) and filtration did not significantly affect the results.

Table 3. Absolute distance error in metres – constant motion; MB model; velocity filtration.

Filter	Δ_p less than [m]							
	0.05	0.1	0.15	0.2	0.3	0.4	0.5	0.6
H + A_49	0.35	0.64	0.87	1.18	1.58	1.98	2.39	2.81
A_49	0.35	0.64	0.87	1.18	1.58	1.98	2.39	2.81
M_49	0.35	0.64	0.94	1.18	1.58	1.98	2.39	2.90
SG_49	0.35	0.71	0.94	1.18	1.58	1.98	2.39	2.90
A_25	0.35	0.64	0.94	1.18	1.58	1.98	2.39	2.90
M_25	0.35	0.64	0.94	1.18	1.58	1.98	2.39	2.81
Raw	0.35	0.64	0.94	1.18	1.58	2.06	2.47	2.90
	Distance travelled [m]							

Table 3 shows that only the filtration of velocity (or only the filtration of acceleration – they show similar results) did not give the expected improvement. However, it is possible not only to filter separately the velocity or acceleration data, but also both data one after another.

Table 4 shows the results after speed filtration but after the pre-filtration of acceleration with a moving-average filter with a window width of seven samples. When interpreting the values from this table, the double filtration (of acceleration and speed) improved the final results, but it also gave better results for a longer period for the A_7 filtration.

Table 4. Absolute distance error in metres – constant motion; MB model; acceleration pre-filtration with A_7 and speed filtration.

Filter	Δ_p less than [m]							
	0.05	0.1	0.15	0.2	0.3	0.4	0.5	0.6
A_7	0.35	0.64	0.94	1.25	1.66	2.14	2.55	2.98
A_13	0.35	0.64	0.94	1.18	1.66	2.14	2.55	2.98
A_25	0.35	0.64	0.94	1.18	1.66	2.06	2.47	2.90
A_49	0.35	0.64	0.94	1.18	1.66	2.06	2.47	2.98
M_25	0.35	0.64	0.94	1.18	1.66	2.06	2.47	2.98
M_49	0.35	0.64	0.94	1.18	1.66	2.06	2.47	2.98
Raw	0.35	0.64	0.94	1.18	1.58	2.06	2.47	2.90
Distance travelled [m]								

It was expected that the acceleration of the RC model would oscillate close to zero during constant motion. However, the amplitude of the oscillation can be too large or the oscillation can be moved to a non-zero value. This phenomenon may cause either underestimation or overestimation of the velocity during constant motion. It is possible to reduce the effect of this phenomenon by using thresholding. This process is designed to change the acceleration values to zero during constant motion when the value of acceleration is within the range of the threshold values. The threshold values depend on the accelerometer and must be selected experimentally. Comparing the results from Table 4 and Table 5, it can be concluded that this process significantly improves the accuracy. The best results were achieved for the moving average filter with a window width of seven samples.

Table 5. Absolute distance error in metres – constant motion; MB model; acceleration pre-filtration with A_7, thresholding and speed filtration.

Filter	Δ_p less than [m]							
	0.05	0.1	0.15	0.2	0.3	0.4	0.5	0.6
A_7	0.64	1.02	1.25	1.74	2.30	2.81	3.24	3.65
A_13	0.64	1.02	1.25	1.74	2.22	2.73	3.24	3.57
A_25	0.64	1.02	1.25	1.74	2.22	2.73	3.24	3.57
A_49	0.64	0.94	1.25	1.74	2.22	2.73	3.24	3.57
M_25	0.64	1.02	1.25	1.74	2.22	2.73	3.24	3.57
M_49	0.64	1.02	1.25	1.74	2.22	2.81	3.24	3.57
Raw	0.64	0.94	1.18	1.58	2.06	2.47	2.90	3.32
Distance travelled [m]								

The filtration process flattens the filtered signal (here the acceleration and velocity), and therefore the final values that are obtained can be understated. The degree of flattening depends

on the filtration algorithm and the window width (the number of samples that are considered for filtration). This phenomenon can be reduced by adding some constant values or by adding a portion of the filtered signal. The second solution is better if the underestimation is even slightly variable – and here it depends on the value of the acceleration. Therefore, in order to add a part of the signal to itself, the signal is simply multiplied by a constant value α which is within the range of $\langle 1.0; 2.0 \rangle$ (analogically, if the signal is overestimated, the value of α is within the range of $\langle 0.0; 1.0 \rangle$). The accuracy and sensitivity of the accelerometer are limited, which means that the fluctuation of acceleration and sensitivity to sudden changes can modify the α value and that they are dependent on the accelerometer that is used.

Table 6 shows the result after adding the flattening compensation mechanism ($\alpha = 1.3$) to the previous filtration process. This modification increases the accuracy of the object positioning during the constant-motion phase up to 0.7 m (A_7) compared with the raw data.

Table 6. Absolute distance error in metres – constant motion; MB model; acceleration pre-filtration with A_7, thresholding with flattening compensation and speed filtration.

Filter	Δ_p less than [m]							
	0.05	0.1	0.15	0.2	0.3	0.4	0.5	0.6
A_7	0.64	0.94	1.25	1.90	2.55	3.15	3.65	4.06
A_13	0.64	0.94	1.25	1.90	2.47	3.07	3.57	3.98
A_25	0.64	0.94	1.25	1.82	2.39	3.07	3.49	3.98
A_49	0.64	0.94	1.25	1.90	2.47	3.07	3.57	3.98
M_25	0.64	0.94	1.25	1.90	2.39	3.07	3.57	3.98
M_49	0.64	0.94	1.25	1.90	2.47	3.07	3.57	3.98
Raw	0.64	0.94	1.18	1.58	2.06	2.47	2.90	3.32
Distance travelled [m]								

3.2. Acceleration phase

The thresholding and flattening compensation mechanisms are used during the entire period of movement in order to make the filtration process universal. These filtration methods are described in Subsection 3.1. Table 7 shows the relationship between the absolute position error and the

Table 7. Absolute distance error in metres – accelerated motion; MB model; acceleration pre-filtration with A_7, thresholding and speed filtration.

Filter	Δ_p less than [m]							
	0.05	0.1	0.15	0.2	0.3	0.4	0.5	0.6
A_7	1.08	1.31	1.49	1.88	2.21	2.48	2.77	3.06
A_13	1.08	1.31	1.49	1.88	2.21	2.48	2.77	3.06
A_25	1.08	1.31	1.56	1.88	2.21	2.55	2.77	3.06
A_49	1.13	1.37	1.56	1.88	2.21	2.55	2.84	3.06
M_25	1.08	1.31	1.56	1.88	2.21	2.48	2.77	3.06
M_49	1.08	1.31	1.56	1.88	2.21	2.48	2.77	3.06
Raw	0.97	1.25	1.43	1.75	2.01	2.28	2.48	2.77
Distance travelled [m]								

distance travelled during the accelerated-motion phase. The A_49 filtration was characterised by a long-term accuracy compared with the other filters. Compared with the analogous table for the constant-motion phase (Table 5), the larger window width produced better results during the acceleration.

In order to observe how a rapid increase in speed affected the operation of the filters, Table 8 shows the results for the accelerated motion of the MA model. By interpreting the data from the table, the best results in the long-term were also achieved for the A_49 filtration, whereas for the A_7 filtration the results were only slightly worse. The results for the filtration with additionally used the flattening compensation method are presented in Table 9. The flattening compensation process reduced twice the absolute distance error and made it possible to travel a distance of 4.95 m with a distance error less than 0.3 m.

Table 8. Absolute distance error in metres – accelerated motion; MA model; acceleration pre-filtration with A_7, thresholding and speed filtration.

Filter	Δp less than [m]							
	0.05	0.1	0.15	0.2	0.3	0.4	0.5	0.6
A_7	0.99	1.76	2.41	2.93	3.46	4.20	4.76	4.95
A_13	0.84	1.76	2.41	2.75	3.46	4.01	4.57	4.95
A_25	0.84	1.76	2.41	2.75	3.46	4.01	4.57	4.95
A_49	1.14	1.76	2.41	2.75	3.46	4.20	4.76	4.95
M_25	0.84	1.76	2.41	2.75	3.46	4.01	4.57	4.95
M_49	0.84	1.76	2.41	2.75	3.46	4.01	4.57	4.95
Raw	0.84	1.60	2.08	2.41	3.10	3.82	4.38	4.95
Distance travelled [m]								

Table 9. Absolute distance error in metres – accelerated motion; MA model; acceleration pre-filtration with A_7, thresholding with flattening compensation and speed filtration.

Filter	Δp less than [m]							
	0.05	0.1	0.15	0.2	0.3	0.4	0.5	0.6
A_7	1.60	2.75	3.46	4.01	4.95	–	–	–
A_13	1.60	2.75	3.46	3.82	4.95	–	–	–
A_25	1.60	2.75	3.46	3.82	4.95	–	–	–
A_49	1.76	2.93	3.46	4.20	4.95	–	–	–
M_25	1.44	2.75	3.28	3.82	4.95	–	–	–
M_49	1.60	2.75	3.28	3.82	4.95	–	–	–
Raw	0.84	1.60	2.08	2.41	3.10	3.82	4.38	4.95
Distance travelled [m]								

4. Conclusion

This paper shows that short-term indoor positioning is possible using the MEMS sensors that smartphones are equipped with and fundamental filters that are characterised by a low computational complexity. For the constant-motion phase of movement, the final result for the

moving average filter with a window width of seven samples (A_7) was 0.7 m better in comparison to that with no filtration, which had a position accuracy of 0.7 m (after moving by more than 4 m). The improvement in relation to the accelerated motion was greater and was equal to 1.85 m with a position accuracy of 0.3 m using A_49 (after movement of almost 5 m).

Smart city and autonomous driving requires many independent systems for object positioning because each piece of position information is useful. MEMS sensors can provide information about the object shift. When location is performed (the process of setting the position on the map), then the superior (or upper) decision system can allow the further movement of an object, even if there is no image information (the object is hidden by trees, other objects or is behind corners). The superior system can use the information about the direction and speed of the movement as well as the delay in the filtration and the accuracy of the INS obtained using MEMS sensors to determine the safe time (or safe area) in which the object can move. It should be emphasised that although INS is an additional positioning subsystem due to the accumulation of errors in time, its advantage is its very fast data rate, which, in turn, enables to increase the precision of other positioning subsystems between their subsequent readings.

This paper's aim was to serve as a compendium of knowledge that would enable to use the data from the accelerometer, gyroscope and magnetometer by positioning algorithms. Our research on the fundamental filters answers the question about how long (how far) an object can navigate without a video system with the use of only an INS subsystem. It shows that it is possible to use a smartphone as the device to position vehicles with limited accuracy, which is sufficient in an indoor environment in which the objects are located on the basis of a video analysis.

Acknowledgements

This work was supported by the Ministry of Science and Higher Education funding for young researchers statutory activities. BKMN 2018.

References

- [1] Grzechca, D., Wrobel, T., Bielecki, P. (2014). Indoor Location and Identification of Objects with Video Surveillance System and WiFi Module. *IEEE*, 171–174.
- [2] Polańczyk, M., Strzelecki, M., Ślot, K. (2013). Obstacle Avoidance Procedure and Lee Algorithm Based Path Replanner for Autonomous Mobile Platforms. *International Journal of Electronics and Telecommunications*, 59(1), 85–91.
- [3] Chruszczyk, Ł., Zając, A. (2016). Comparison of Indoor/Outdoor, RSSI-Based Positioning Using 433, 868 or 2400 MHz ISM Bands. *International Journal of Electronics and Telecommunications*, 62(4), 395–399.
- [4] De Angelis, A., Nilsson, J., Skog, I., Händel, P., Carbone, P. (2010). Indoor Positioning by Ultrawide Band Radio Aided Inertial Navigation. *Metrol. Meas. Syst.*, 17(3), 447–460.
- [5] Kamiński, Ł., Bruniecki, K. (2012). Mobile Navigation System for Visually Impaired Users in the Urban Environment. *Metrol. Meas. Syst.*, 19(2), 245–256.
- [6] Pitas, I., Venetsanopoulos, A.N. (1990). *Nonlinear Digital Filters*. Springer US, Boston, MA.
- [7] Smith, S.W. (1997). *The scientist and engineer's guide to digital signal processing*. 1st ed California Technical Pub, San Diego, Calif.
- [8] Gallagher, N., Wise, G. (1981). A theoretical analysis of the properties of median filters. *IEEE Transactions on Acoustics, Speech, and Signal Processing*, 29 (6), 1136–1141.

- [9] de Oliveira, M., Araujo, N., da Silva, R., da Silva, T., Epaarachchi, J. (2018). Use of Savitzky–Golay Filter for Performances Improvement of SHM Systems Based on Neural Networks and Distributed PZT Sensors. *Sensors*, 18(2), 152.
- [10] Pearson, R.K., Neuvo, Y., Astola, J., Gabbouj, M. (2016). Generalized Hampel Filters. *EURASIP Journal on Advances in Signal Processing*, (1), 87.
- [11] STMicroelectronics (2014). Tilt measurement using a low-g 3-axis accelerometer.
- [12] Michael J. Caruso (1997). Applications of Magnetoresistive Sensors in Navigation Systems.
- [13] Chruszczyk, Ł., Zając, A., Grzechca, D. (2016). Comparison of 2.4 and 5 GHz WLAN Network for Purpose of Indoor and Outdoor Location. *International Journal of Electronics and Telecommunications*, 62(1), 71–79.
- [14] Botta, M., Simek, M. (2013). Adaptive Distance Estimation Based on RSSI in 802.15.4 Network. *Radioengineering*, 22(4), 1162–1168.
- [15] Zhu, X., Feng, Y. (2013). RSSI-based Algorithm for Indoor Localization. *Communications and Network*, 05 (02), 37–42.
- [16] Lagarias, J.C., Reeds, J.A., Wright, M.H., and Wright, P.E. (1998). Convergence Properties of the Nelder–Mead Simplex Method in Low Dimensions. *SIAM Journal on Optimization*, 9(1), 112–147.